Electrochemical, Spectroscopic, and Computational Investigation of a Series of Polypyridyl Ruthenium(II) Complexes: Characterization of Reduced States

Nicolas Queyriaux, Charlène Esmieu, Arvind K Gupta, Laure Vendier, Sascha Ott, Maylis Orio, Leif Hammarström

Synthesis, structural characterization and electrochemical behavior of a series of polypyridyl ruthenium(II) complexes

N. Queyriaux,[1,2]* C. Esmieu,[1] A. K. Gupta,[1] L. Vendier,[2] S. Ott[1] M. Orio[3] and L. Hammarström[1]*

1 - Department of Chemistry, Ångström Laboratories Uppsala University, Box 523, 751 20 Uppsala, Sweden

2 – CNRS, LCC (Laboratoire de Chimie de Coordination), 31077 Toulouse, France

3 – Aix Marseille Univ., CNRS, Centrale Marseille, iSm2, 13397 Marseille, France.

e-mail: nicolas.queyriaux@lcc-toulouse.fr / leif.hammarstrom@kemi.uu.se

Abstract.

A series of polypyridyl ruthenium(II) complexes has been synthesized and characterized by ^{1}H-NMR, electronic absorption and voltammetric techniques. Among this series, hexafluorophosphate salts of eight ruthenium(II) complexes were newly prepared. Due to the well-known ability of this class of compounds to assist electro- and photocatalytic reductive processes (such as the reduction of CO_2, H^+ and $NAD(P)^+$ models), a particular attention has been paid to investigate the nature of their one- and two-electron reduced species through computational and spectroscopic techniques.

Introduction.

Polypyridyl ruthenium(II) complexes featuring the general formula $[Ru^{II}(N\hat{}N\hat{}N)(N\hat{}N)X]^{n+}$ (N^N^N and N^N = substituted tridentate and bidentate polypyridyl ligands, respectively X = monodentate ligand, n = 1 or 2) have attracted much interest due to their large scope of applications. Upon absorption of a photon of suitable energy, promotion of an electron in a singlet metal-to-ligand charge transfer (^{1}MLCT) excited state is observed. Following a fast intersystem crossing to the related triplet state (^{3}MLCT), non-radiative transition to a triplet metal-centered state (^{3}MC) may occur. Due to its antibonding nature, populating this excited state typically induces dissociation of the monodentate X ligand.[1, 2] This specific photochemical behavior, distinct from the textbook one observed in the case of $[Ru(bpy)_3]^{2+}$, has been widely exploited in photodynamic therapy,[3, 4] light-induced drug-release[5-7] and molecular photo-actuation[8, 9]. Alternatively, the combination of a robust polypyridine coordination sphere and a relatively labile X ligand has led to the frequent use of representative members of this family of compounds to serve as efficient photo- or electro-catalysts in either oxidative (water oxidation[10-12]) or reductive (reduction of CO_2,[13-17] protons[12, 18] or $NAD(P)^+$ models[19]) processes.

Mechanistic studies carried out on the electro-assisted reduction of CO_2 by certain complexes from this family of compounds generally raise the question of the nature of the reduced species capable of interacting with a CO_2 molecule.[13, 20, 21] How many electrons are needed by the catalyst to allow the coordination of the CO_2 molecule and thus initiate its activation through bending? At present, two mechanisms have been proposed depending on the steric hindrance directed toward the metal center.

In the absence of any significant on-metal steric hindrance, Meyer and coworkers. proposed a catalytic mechanism initiated by an electrochemical EEC-type sequence (with E, an electrochemically induced electron transfer and C, a homogeneous chemical process).[21] Two successive reductions are thus necessary to allow dissociation of the acetonitrile ligand and coordination of a CO_2 molecule. A rapid electronic reorganization of this adduct is generally suggested, resulting in a metallocarboxylate species in which most of the electron density derived from the two reductions is localized on the CO_2 ligand. Alternatively, some of us have shown the impact of a simple modification of the polypyridyl ligand set. The on-metal steric hindrance induced by the introduction of a methyl group on the bipyridine ligand was able to dramatically facilitate the formation of a highly reactive five-coordinate species and thus alter the activation mechanism of the CO_2 molecule, resulting in an ECE sequence.[13] These mechanistic propositions are based on a careful analysis of the electrochemical behavior of the complexes in the presence and absence of their substrate, carbon dioxide. Spectroscopic observations of key one- and two-electron reduced intermediates under electrocatalytically-relevant conditions are, however, still needed.

In this context, we synthesized a series of polypyridyl ruthenium(II) complexes displaying the general formula $[Ru^{II}(N\text{^}N\text{^}N)(N\text{^}N)(MeCN)]^{2+}$. A detailed description of their spectroscopic and electrochemical properties is provided. The electronic structures and main spectroscopic features (UV-Vis & EPR) of the one- and two electron reduced species of **1-MeCN**, a representative complex within the series, was investigated to help future mechanistic studies using coupled spectroelectrochemical (SEC) methods or transient absorption spectroscopy (TAS) techniques.

Experimental.

Materials.

All solvents were reagent-grade and all materials were used as received unless otherwise stated. $RuCl_3.3H_2O$, triethylamine (TEA), 2,2′:6′,2″-terpyridine (tpy), 4,4′,4″-tri-^{t}butyl-2,2′:6′,2″-terpyridine (^{t}Bu$_3$-tpy), 2,2′-bipyridine (bpy), 4,4′-dimethyl-2,2′-bipyridine (Me$_2$-bpy), 1,10-phenanthroline (phen), 4,4′-di-^{t}butyl-2,2′-bipyridine (^{t}Bu$_2$-bpy), 2,2′-biquinoline (bqn) and 4,4′- dimethoxy-2,2′-bipyridine (MeO$_2$-bpy) were purchased from Sigma-Aldrich. Ru(tpy)Cl$_3$[22] and Ru(^{t}Bu$_3$-tpy)Cl$_3$[23] were synthesized as previously described.

Synthesis.

General Procedure for [Ru^{II}(N^N^N)(N^N)Cl](PF$_6$). The appropriate Ru(N^N^N)Cl$_3$ ruthenium precursor was refluxed overnight with one equivalent of the desired bidentate N^N ligand, in the presence of LiCl (5.0 equivalents) and TEA (1.5 equivalents) in deaerated EtOH/H_2O mixture (100 mL, 3:1). Solvents were evaporated under reduced pressure and 20 mL of water added. Precipitation of the complex was triggered by the dropwise addition of 2 mL of a saturated aqueous solution of NH_4PF_6 and the resulting suspension was stirred for 30 min. The precipitate was collected, thoroughly washed with H_2O. The crude product was then subjected to a two-step purification procedure. Firstly, purified by chromatography on alumina (toluene / acetonitrile, 50:50), the desired compound was then

eluted from a second chromatography on silica (acetone / 10 % saturated NH_4PF_6 solution, 98:2). The major purple band was collected and concentrated under reduced pressure precipitating out the desired product, which was collected, washed with H_2O, and dried under vacuum overnight.

[Ru^{II}(tpy)(bpy)Cl](PF$_6$) **(1-Cl)**. R = 93%.

^{1}H NMR (400 MHz, acetone-*d6*): δ 10.34 (dd, J = 5.7, 1.6 Hz, 1H), 8.88 (d, J = 7.8 Hz, 1H), 8.75 (d, J = 8.1 Hz, 2H), 8.67 – 8.56 (m, 3H), 8.39 (td, J = 7.8, 1.6 Hz, 1H), 8.21 (t, J = 8.1 Hz, 1H), 8.07 (dd, J = 8.9, 5.7 Hz, 1H), 8.00 (td, J = 7.4, 1.5 Hz, 2H), 7.87 – 7.75 (m, 3H), 7.59 (dd, J = 5.7, 1.3 Hz, 1H), 7.40 (ddd, J = 7.4, 5.5, 1.3 Hz, 2H), 7.11 (ddd, J = 7.3, 5.7, 1.3 Hz, 1H). **ESI-MS**: m/z: 525.9 [M-PF6]$^+$. Characterizations are in good agreement with previous report.[24]

[Ru(^{t}Bu$_3$-tpy)(bpy)Cl](PF$_6$) **(2-Cl)**. R = 72%.

^{1}H NMR (400 MHz, acetone-*d6*): δ 10.35 (d, J = 5.6 Hz, 1H), 8.87 – 8.84 (m, 3H), 8.72 (d, J = 1.8 Hz, 2H), 8.59 (d, J = 8.0 Hz, 1H), 8.35 (ddd, J = 8.2, 7.5, 1.6 Hz, 1H), 8.04 (ddd, J = 7.5, 5.6, 1.3 Hz, 1H), 7.79 (ddd, J = 8.0, 7.5, 1.4 Hz, 1H), 7.67 (d, J = 5.9 Hz, 2H), 7.57 (dd, J = 5.7, 0.6 Hz, 1H), 7.38 (dd, J = 5.9, 1.8 Hz, 2H), 7.08 (ddd, J = 7.5, 5.7, 1.4 Hz, 1H), 1.62 (s, 9H), 1.36 (s, 18H). **ESI-MS**: m/z: 694.3 [M-PF6]$^+$. Characterizations are in good agreement with previous report.[10]

[Ru(tpy)(Me$_2$-bpy)Cl](PF$_6$) **(3-Cl)**. R = 96%.

^{1}H NMR (400 MHz, acetone-*d6*): δ 10.13 (d, J = 5.7 Hz, 1H), 8.76 – 8.70 (m, 3H), 8.61 (td, J = 8.1, 1.1 Hz, 2H), 8.46 (d, J = 1.7 Hz, 1H), 8.18 (t, J = 8.1 Hz, 1H), 7.99 (td, J = 7.7, 1.5 Hz, 2H), 7.91 (dd, J = 5.8, 1.0 Hz, 1H), 7.83 (ddd, J = 5.5, 1.4, 0.7 Hz, 2H), 7.40 (ddd, J = 7.5, 5.5, 1.3 Hz, 2H), 7.34 (d, J = 5.9 Hz, 1H), 6.93 (dd, J = 5.9, 1.1 Hz, 1H), 2.80 (s, 3H), 2.36 (s, 3H). **ESI-MS**: m/z: 554.0 [M-PF6]$^+$. Characterizations are in good agreement with previous report.[20]

[Ru(^{t}Bu$_3$-tpy)(Me$_2$-bpy)Cl](PF$_6$) **(4-Cl)**. R = 75%.

^{1}H NMR (400 MHz, acetone-*d6*): δ 10.11 (d, J = 5.7 Hz, 1H), 8.79 (s, 2H), 8,69 (s, 1H), 8.67 (d, J = 2.0 Hz, 2H), 8.42 (s, 1H), 7.85 (d, J = 5.8 Hz, 1H), 7.64 (d, J = 5.9 Hz, 2H), 7.35 (dd, J = 5.9, 2.0 Hz, 2H), 7.29 (d, J = 5.9 Hz, 1H), 6.88 (d, J = 6.0 Hz, 1H), 2.34 (s, 3H), 2.06 (s, 3H), 1.59 (s, 9H), 1.33 (s, 18H). **ESI-MS**: m/z: 722.3 [M-PF6]$^+$. Characterizations are in good agreement with previous report.[25]

[Ru(^{t}Bu$_3$-tpy)(phen)Cl](PF$_6$) **(5-Cl)**. R = 68%.

^{1}H NMR (400 MHz, acetone-*d6*): δ 10.35 (dd, J = 5.6, 0.7 Hz, 1H), 8.89 – 8.82 (m, 3H), 8.72 (d, J = 1.6 Hz, 2H), 8.59 (d, J = 8.0 Hz, 1H), 8.35 (ddd, J = 8.2, 7.7, 1.6 Hz, 1H), 8.04 (ddd, J = 7.5, 5.6, 1.3 Hz, 1H), 7.79 (ddd, J = 8.2, 7.7, 1.4 Hz, 1H), 7.67 (d, J = 5.9 Hz, 2H), 7.57 (dd, J = 5.7, 0.6 Hz, 1H), 7.38 (dd, J = 5.9, 2.1 Hz, 2H), 7.08 (ddd, J = 7.3, 5.8, 1.4 Hz, 1H), 1.62 (s, 9H), 1.36 (s, 18H). **ESI-MS**: m/z: 718.3 [M-PF6]$^+$.

[Ru(^{t}Bu$_3$-tpy)(^{t}Bu$_2$-bpy)Cl](PF$_6$) **(6-Cl)**. R = 55%.

^{1}H NMR (400 MHz, acetone-*d6*): δ 10.21 (d, J = 6.0 Hz, 1H), 8.88 (d, J = 1.8 Hz, 1H), 8.82 (s, 2H), 8.68 (d, J = 1.8 Hz, 2H), 8.62 (d, J = 2.0 Hz, 1H), 8.06 (dd, J = 6.0, 2.0 Hz, 1H), 7.62 (d, J = 6.0 Hz, 2H), 7.41 – 7.29 (m, 3H), 7.05 (dd, J = 6.2, 2.1 Hz, 1H), 1.60 (s, 9H), 1.57 (s, 9H), 1.34 (s, 18H), 1.22

(s, 9H). **ESI-MS**: m/z: 806.52 $[M\text{-}PF6]^+$. Characterizations are in good agreement with previous report.[10]

[Ru(^{t}Bu$_3$-tpy)(bqn)Cl](PF$_6$) **(7-Cl)**. R = 60%.

^{1}H NMR (400 MHz, acetone-*d6*): δ 9.86 (d, J = 8.9 Hz, 1H), 9.06 (d, J = 8.9 Hz, 1H), 8.95 (d, J = 8.8 Hz, 1H), 8.85 (s, 2H), 8.78 (d, J = 8.9 Hz, 1H), 8.66 (d, J = 2.1 Hz, 2H), 8.38 – 8.29 (m, 2H), 7.93 – 7.86 (m, 2H), 7.83 (ddd, J = 8.6, 6.9, 1.6 Hz, 1H), 7.77 (d, J = 6.0 Hz, 2H), 7.50 (ddd, J = 8.0, 7.0, 1.0 Hz, 1H), 7.38 (dd, J = 6.0, 2.1 Hz, 2H), 7.24 (ddd, J = 8.5, 5.3, 1.5 Hz, 1H), 6.96 (d, J = 8.9 Hz, 1H), 1.64 (s, 9H), 1.33 (s, 18H). **ESI-MS**: m/z: 794.4 $[M\text{-}PF6]^+$.

[Ru(^{t}Bu$_3$-tpy)(MeO$_2$-bpy)Cl](PF$_6$) **(8-Cl)**. R = 64%.

^{1}H NMR (400 MHz, acetone-*d6*): δ 10.07 (d, J = 6.5 Hz, 1H), 8.81 (s, 2H), 8.69 (d, J = 2.0 Hz, 2H), 8.44 (d, J = 2.7 Hz, 1H), 8.18 (d, J = 2.8 Hz, 1H), 7.76 (d, J = 5.9 Hz, 2H), 7.68 (dd, J = 6.5, 2.7 Hz, 1H), 7.40 (dd, J = 5.9, 2.1 Hz, 2H), 7.18 (d, J = 6.6 Hz, 1H), 6.66 (dd, J = 6.6, 2.8 Hz, 1H), 4.24 (s, 3H), 3.89 (s, 3H), 1.61 (s, 9H), 1.37 (s, 18H). **ESI-MS**: m/z: 754.3 $[M\text{-}PF6]^+$.

General Procedure for [Ru^{II}(N^N^N)(N^N)(MeCN)](PF$_6$)$_2$. Appropriate $[Ru^{II}(N^N^N)(N^N)Cl](PF_6)$ complex was dissolved in degassed $MeCN/H_2O$ mixture (2:1, 60 mL) and refluxed under argon overnight. Acetonitrile was evaporated under reduced pressure and a few drops of a saturated aqueous solution of NH_4PF_6 were added to the solution. The resulting suspension was stirred for 30 min. The typically bright orange precipitate was collected, thoroughly washed with H_2O and dried under vacuum overnight.

[Ru(tpy)(bpy)(MeCN)](PF$_6$)$_2$ **(1-MeCN)**. **(**R = 91%).

^{1}H NMR (400 MHz, acetone-*d6*): δ 9.91 (d, J = 5.6 Hz, 1H), 8.93 (d, J = 8.3 Hz, 1H), 8.89 (d, J = 8.1 Hz, 2H), 8.74 (d, J = 8.0 Hz, 2H), 8.68 (d, J = 8.2 Hz, 1H), 8.48 (m, 2H), 8.17 (td, J = 8.0, 1.4 Hz, 2H), 8.11 (ddd, J = 7.0, 5.6, 1.1 Hz, 1H), 8.02 – 7.93 (m, 3H), 7.64 (d, J = 5.8 Hz, 1H), 7.54 (ddd, J = Hz, 2H), 7.25 (ddd, J = 7.2, 5.8, 1.1 Hz, 1H). **ESI-MS**: m/z: 265.8 $[M\text{-}2PF6]^{2+}$. Characterizations are in good agreement with previous report.[2]

[Ru(^{t}Bu$_3$-tpy)(bpy)(MeCN)](PF$_6$)$_2$ **(2-MeCN)**. R = 79%.

^{1}H NMR (400 MHz, acetone-*d6*): δ 9.91 (d, J = 5.5 Hz, 1H), 8.99 (s, 2H), 8.92 (d, J = 8.2 Hz, 1H), 8.84 (d, J = 1.9 Hz, 2H), 8.67 (d, J = 8.1 Hz, 1H), 8.45 (td, J = 7.9, 1.5 Hz, 1H), 8.09 (ddd, J = 1.3, 5.6, 7.0 Hz, 1H), 7.95 (td, J = 7.9, 1.4 Hz, 1H), 7.84 (d, J = 5.9 Hz, 2H), 7.57 (d, J = 5.0 Hz, 1H), 7.50 (dd, J = 5.9, 2.1 Hz, 2H), 7.21 (ddd, J = 7.3, 5.7, 1.3 Hz, 1H), 1.63 (s, 9H), 1.37 (s, 18H). **ESI-MS**: m/z: 350.0 $[M\text{-}2PF6]^{2+}$.

[Ru(tpy)(Me$_2$-bpy)(MeCN)](PF$_6$)$_2$ **(3-MeCN)**. R = 77%.

^{1}H NMR (400 MHz, acetone-*d6*): δ 9.67 (d, J = 5.7 Hz, 1H), 8.84 (d, J = 8.1 Hz, 2H), 8.77 (s, 1H), 8.70 (d, J = 8.0 Hz, 2H), 8.52 (s, 1H), 8.43 (t, J = 8.1 Hz, 1H), 8.14 (td, J = 7.9, 1.1 Hz, 2H), 7.96 (d, J = 5.2 Hz, 2H), 7.91 (d, J = 5.2 Hz, 1H), 7.57 – 7.45 (t, J = 6.3 Hz, 2H), 7.38 (d, J = 5.9 Hz, 1H), 7.04 (d, J = 5.5 Hz, 1H), 2.38 (s, 3H), 2.28 (s, 3H). **ESI-MS**: m/z: 279.8 $[M\text{-}2PF6]^{2+}$. Characterizations are in good agreement with previous report.[26]

[Ru(^{t}Bu$_3$-tpy)(Me$_2$-bpy)(MeCN)](PF$_6$)$_2$ **(4-MeCN)**. R = 74%.

^{1}H NMR (400 MHz, acetone-*d6*): δ 9.70 (d, J = 5.7 Hz, 1H), 8.97 (s, 2H), 8.84 (d, J = 1.8 Hz, 2H), 8.80 (s, 1H), 8.54 (s, 1H), 7.93 (d, J = 4.9 Hz, 1H), 7.84 (d, J = 5.9 Hz, 2H), 7.51 (dd, J = 5.9, 2.1 Hz, 2H), 7.35 (d, J = 5.9 Hz, 1H), 7.03 (d, J = 4.9 Hz, 1H), 2.40 (s, 3H), 2.32 (s, 3H), 1.62 (s, 9H), 1.37 (s, 18H). **ESI-MS**: m/z: 364.0 $[M-2PF6]^{2+}$. Characterizations are in good agreement with previous report.[25]

[Ru(^{t}Bu$_3$-tpy)(phen)(MeCN)](PF6)$_2$ **(5-MeCN)**. R = 79%.

^{1}H NMR (400 MHz, acetone-*d6*): δ 10.26 (dd, J = 5.2, 1.2 Hz, 1H), 9.06 (dd, J = 8.3, 1.2 Hz, 1H), 9.03 (s, 2H), 8.85 (d, J = 1.8 Hz, 2H), 8.55 (dd, J = 8.2, 1.1 Hz, 1H), 8.49 (d, J = 8.9 Hz, 1H), 8.45 (dd, J = 8.3, 5.2 Hz, 1H), 8.29 (d, J = 8.9 Hz, 1H), 7.94 (dd, J = 5.3, 1.2 Hz, 1H), 7.72 (d, J = 5.9 Hz, 2H), 7.55 (dd, J = 8.2, 5.3 Hz, 1H), 7.34 (dd, J = 5.9, 2.1 Hz, 2H), 1.66 (s, 9H), 1.33 (s, 18H). **ESI-MS**: m/z: 362.0 $[M-2PF6]^{2+}$.

[Ru(^{t}Bu$_3$-tpy)(^{t}Bu$_2$-bpy)(MeCN)](PF$_6$)$_2$ **(6-MeCN)**. R = 77%.

^{1}H NMR (400 MHz, acetone-*d6*): δ 9.79 (d, J = 6.0 Hz, 1H), 9.02 – 8.94 (m, 3H), 8.84 (d, J = 2.0 Hz, 2H), 8.73 (d, J = 1.9 Hz, 1H), 8.09 (dd, J = 6.0, 2.0 Hz, 1H), 7.80 (d, J = 5.9 Hz, 2H), 7.50 (dd, J = 5.9, 2.0 Hz, 2H), 7.39 (d, J = 6.1 Hz, 1H), 7.19 (dd, J = 6.1, 2.0 Hz, 1H), 1.63 (s, 9H), 1.59 (s, 9H), 1.37 (s, 18H), 1.25 (s, 9H). **ESI-MS**: m/z: 406.1 $[M-2PF6]^{2+}$.

[Ru(^{t}Bu$_3$-tpy)(bqn)(MeCN)](PF$_6$)$_2$ **(7-MeCN)**. R = 68%.

^{1}H NMR (400 MHz, acetone-*d6*): δ 9.19 (d, J = 8.8 Hz, 1H), 9.10 (d, J = 8.8 Hz, 1H), 9.06 – 8.98 (m, 3H), 8.93 (d, J = 8.9 Hz, 1H), 8.81 (d, J = 2.1 Hz, 2H), 8.58 (d, J = 8.8 Hz, 1H), 8.48 (dd, J = 8.1, 1.3 Hz, 1H), 8.10 (ddd, J = 8.7, 5.4, 1.5 Hz, 1H), 8.00 (m, 2H), 7.94 (d, J = 5.9 Hz, 2H), 7.58 (ddd, J = 0.7, 7.5, 7.9 Hz, 1H), 7.52 (dd, J = 6.0, 2.1 Hz, 2H), 7.33 (ddd, J = 8.7, 6.9, 1.5 Hz, 1H), 6.99 (d, J = 8.9 Hz, 1H), 1.66 (s, 9H), 1.33 (s, 18H). **ESI-MS**: m/z: 400.0 $[M-2PF6]^{2+}$.

[Ru(^{t}Bu$_3$-tpy)(MeO$_2$-bpy)(MeCN)](PF$_6$)$_2$ **(8-MeCN)**. R = 69%.

^{1}H NMR (400 MHz, acetone-*d6*): δ 9.62 (d, J = 6.4 Hz, 1H), 8.96 (s, 2H), 8.82 (d, J = 1.9 Hz, 2H), 8.50 (d, J = 2.7 Hz, 1H), 8.24 (d, J = 2.8 Hz, 1H), 7.91 (d, J = 5.9 Hz, 2H), 7.65 (dd, J = 6.5, 2.7 Hz, 1H), 7.53 (dd, J = 5.9, 2.1 Hz, 2H), 7.24 (d, J = 6.6 Hz, 1H), 6.74 (dd, J = 6.6, 2.8 Hz, 1H), 4.24 (s, 3H), 3.91 (s, 3H), 1.62 (s, 9H), 1.38 (s, 18H). **ESI-MS**: m/z: 380.0 $[M-2PF6]^{2+}$.

Physical measurements.

^{1}H-NMR spectra were recorded in acetone-*d6* using a JEOL 400 MHz spectrometer at 293 K. The chemical shifts given in ppm are internally referenced to the residual acetone-*d6* solvent signal (2.05 ppm).[27] Mass spectrometry (MS) spectra were obtained using a Thermo LCQ Deca XP Max with electrospray ionization. UV-Vis absorption spectra were recorded in spectroscopic-grade acetonitrile using a Varian Cary 50 spectrophotometer with 1 nm resolution.

Single crystal X-ray Crystallography.

For complex **4-Cl**, reflections were collected on a Bruker APEXII CCD diffractometer using graphite monochromated MoKα radiation (λ = 0.71073 Å). Crystals were mounted on the loop. Data reduction

was performed with SAINT. Absorption corrections for the area detector were performed using SADABS. Structures were determined by direct methods and refined by least-squares methods on F2 using the SHELX suit of programs. Non-hydrogen atoms were refined anisotropically. Hydrogen atoms were constrained in geometrical positions to their parent atoms unless otherwise specified.

For complex **1-Cl**, data were collected at low temperature (100 K) on a Bruker Kappa Apex II diffractometer using a microsource with a Mo-Kα radiation (λ = 0.71073Å) and equipped with an Oxford Cryosystems Cryostream Cooler Device. The structures have been solved by Direct Methods using SHELXS97, and refined by means of least-squares procedures on a F2 with the aid of SHELXL2016, included in the software package WinGX version 1.637. The Atomic Scattering Factors were taken from International tables for X-Ray Crystallography. All hydrogens atoms were placed geometrically, and refined by using a riding model. All non-hydrogens atoms were anisotropically refined.

Electrochemistry.

Cyclic voltammetry (CV) experiments were performed on an Autolab PGSTAT100 potentiostat controlled with GPES 4.9 software. Measurements were carried out in a typical three-electrode configuration associating a glassy carbon disc (GC) as the working electrode, a platinum wire as auxiliary electrode and a $Ag/AgNO_3$ reference electrode.[28] Unless otherwise stated, CVs were performed on Ar-deareated acetonitrile solution (containing 0.1 M of $^nBu_4NPF_6$ as the supporting electrolyte) typically containing 0.75 mM of each complex. All potentials given in this work are reported with respect to Fc^+/Fc couple, thanks to the addition of ferrocene as an internal standard after each experiment. The potential of the Fc^+/Fc couple was usually found at 0.035 V vs $Ag/AgNO_3$ in acetonitrile.

Electron Paramagnetic Resonance.

Measurements were performed on a Bruker ELEXYS E500 spectrometer using an ER049X SuperX microwave bridge, in a Bruker SHQ0601 cavity equipped with an Oxford Instruments continuous flow cryostat, and using an ITC 503 temperature controller (Oxford Instruments). The Xepr software package from Bruker was used for data acquisition and processing of spectra while g factors were extracted using Easyspin package.

Results and Discussions.

Synthesis.

The Ru^{II}-polypyridyl complexes were synthesized through a typical stepwise procedure.[7] In a first step, $[Ru^{III}(N\hat{}N\hat{}N)Cl_3]$ precursors were prepared by reacting the appropriate N^N^N tridentate ligand with $RuCl_3.3H_2O$. Further introduction of the desired N^N bidentate ligand was then realized by heating both reactants in the presence of LiCl and NEt_3 in an $EtOH/H_2O$ mixture, to yield a range of $[Ru^{II}(N\hat{}N\hat{}N)(N\hat{}N)(Cl)](PF_6)$ complexes (Figure 1A, **1-Cl** to **8-Cl**). Substitution of the chloride

ligand was finally achieved by refluxing the complexes in a CH_3CN/H_2O mixture, thus generating the corresponding acetonitrile-bearing derivatives (Figure 1A, **1-MeCN** to **8-MeCN**). Due to the well-described properties of this family of compounds to undergo photo-induced solvolysis reactions,[29] ^{1}H-NMR spectra were recorded in the dark using deuterated acetone as a poorly coordinating solvent. Complete assignments of the well-dispersed signals are described in the Supplementary Information (Figures S1-S16). In particular, chloride ligand exchange by an acetonitrile molecule can easily be monitored thanks to dramatic shielding of the signal associated with monodentate ligand-directed proton on the bidentate ligands (from 10.07 ppm in **8-Cl** to 9.62 ppm in **8-MeCN**, as an example). Furthermore, ESI-MS spectra confirmed the calculated mass-to-charge ratios of the expected molecular fragments.

Structural characterization.

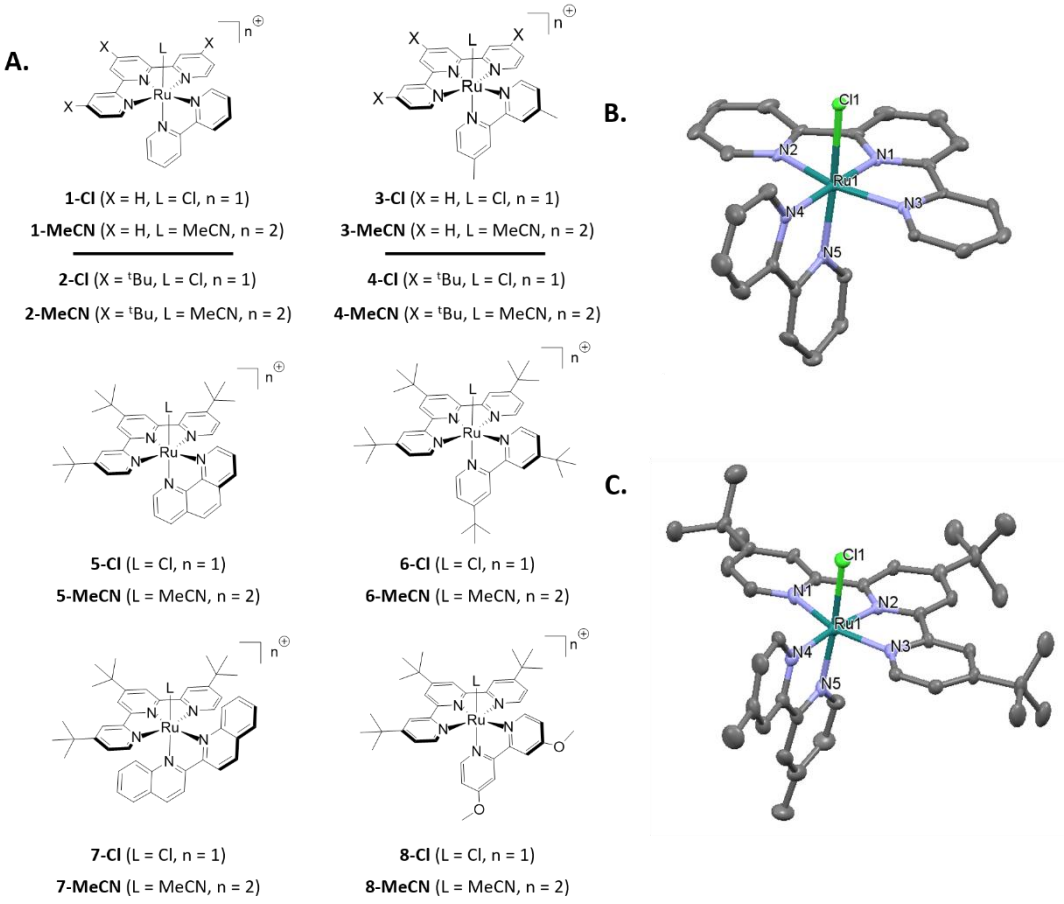

Figure 1. Structures of the Ru^{II}-polypyridyl complexes studied in the present work (A) and molecular structure of **1-Cl** (B) and **4-Cl** (C). Ellipsoids are set at 30% probability; hydrogen atoms, PF_6^- counterions and solvent molecules have been omitted for sake of clarity.

The structure of **1-Cl** and **4-Cl** were determined by X-ray crystallography (Figure 1B-1C). Both complexes display distorted octahedral geometries, with Ru-N bond lengths in the range 1.941(5)-2.074(5) Å and very similar Ru-Cl bond lengths (Table S1 for selected bond lengths and angles). Interestingly the pyridine rings within each bi- or tridentate ligand are not strictly coplanar. In **1-Cl**,

the bidentate ligand features a torsion angle α of 4.40°, the tridentate ligand being characterized by a moderate deviation from planarity with β = 0.40° and β' = 4.03° (mean planes and dihedral angles are defined in the Supporting Information, with the corresponding angle values listed in Table S1). In **4-Cl**, ligands are significantly more "twisted", torsion angles of α = 11.71°, β = 6.59°and β' = 1.61° being calculated.

Electrochemical properties.

The electrochemical behavior of the $[Ru^{II}(N^N^N)(N^N)X]^{n+}$ (X = Cl^-/MeCN, n = 1 / 2) series of compounds were systematically assessed by cyclic voltammetry (CV) and differential pulse voltammetry (DPV) in acetonitrile under inert atmosphere (Table 1 and Figures S17-32 in the Supplementary Information). In the anodic domain, CVs feature a reversible, one-electron electrochemical process assigned to the $Ru^{II/III}$ couple.[30] The potential of this couple is strongly affected by the nature of the monodentate ligand. The replacement of a chloride ligand by acetonitrile typically leads to a 500 mV shift towards more positive potentials (**1-Cl** compared to **1-MeCN**, as an example). In comparison, the polypyridyl ligand set appears to display a smaller influence. Recorded shifts in potential of the $Ru^{II/III}$ couple are indeed in good agreement with the electron-donating/withdrawing ability of the substituents (**1-Cl** compared to **2-Cl** for N^N^N tridentate ligand-based substitution or **2-MeCN** compared to **7-MeCN** for modification of the N^N bidentate ligand) albeit limited to 100 mV as a maximum.

Table 1. Redox potentials of complexes **1-Cl** to **8-Cl** and **1-MeCN** to **8-MeCN** (in V vs Fc+/Fc).

Compound	$E_{1/2,\ ox}$ (ΔEp)	$E_{1/2,\ red\text{-}1}$ (ΔEp)	$E_{1/2,\ red\text{-}2}$ (ΔEp)
1-Cl	+0.40 (83 mV)	-1.83 (98 mV)	-1.98 (83 mV)
1-MeCN	+0.90 (71 mV)	-1.68 (83 mV)	-1.97 (92 mV)
2-Cl	+0.32 (79 mV)	-1.90 (93 mV)	-2.00 (irr.)
2-MeCN	+0.82 (83 mV)	-1.76 (94 mV)	-1.99 (110 mV)
3-Cl	+0.36 (88 mV)	-1.85 (100 mV)	-2.03 (100 mV)
3-MeCN	+0.85 (78 mV)	-1.68 (83 mV)	-2.02 (118 mV)
4-Cl	+0.27 (78 mV)	-1.95 (97 mV)	-2.06 (irr.)
4-MeCN	+0.77 (78 mV)	-1.79 (83 mV)	-2.05 (82 mV)
5-Cl	+0.32 (78 mV)	-1.91 (83 mV)	-2.03 (irr.)
5-MeCN	+0.83 (83 mV)	-1.77 (93 mV)	-1.99 (78 mV)
6-Cl	+0.27 (88 mV)	-1.96 (82 mV)	-2.07 (93 mV)
6-MeCN	+0.77 (83 mV)	-1.79 (87 mV)	-2.05 (130 mV)
7-Cl	+0.40 (78 mV)	-1.47 (88 mV)	-1.83 (irr.)
7-MeCN	+0.87 (89 mV)	-1.34 (83 mV)	-1.84 (71 mV)
8-Cl	+0.21 (78 mV)	-1.98 (91 mV)	-2.07 (irr.)

8-MeCN	+0.70 (94 mV)	-1.81 (104 mV)	-2.05 (114 mV)

irr.: irreversible electrochemical process. In this case, redox potentials are originating from the DPV measurements.

On the other hand, cathodic scans of the series of compounds provided insights on the chemical stability of the electroactive species. All $[Ru^{II}(N^N^N)(N^N)(CH_3CN)]^{2+}$ complexes are initially featuring a quasi-reversible, one-electron reduction characterized by a peak-to-peak difference $\Delta(Ep_a-Ep_c)$ in the 80-100 mV range. A second reductive event is observed at more negative potentials, with a degree of reversibility that varied with the nature of the bidentate ligand. The relatively poor reversibility of this second process has previously been ascribed to the loss of the acetonitrile ligand, generating a five-coordinate species.[20] According to earlier reports, both redox processes have been attributed to ligand-centered reductions.[14, 21, 31] The first reduction can be assigned to the N^N^N ligand, in agreement with related $[Ru^{II}(N^N^N)(N^N)L]^{2+}$ complexes,[ref#] except in complex **7** where the biquinoline ligand is the first to be reduced. These ligand-centered reductive processes are, less affected, compared to the $Ru^{III/II}$ couple, by modifications to the polypyridyl coordination environment. Replacement of the chloride ligand by MeCN shifts the first reduction by only ca. 150 mV, while the second reduction is essentially unaffected (presumably due to Cl^- loss upon reduction, see next paragraph). Substituting the N^N^N tridentate ligand with electron-donating ^{t}Bu groups is responsible for ~100 mV shift towards more negative potentials for the first reduction process (**1-MeCN** compared to **2-MeCN**, as an example), whereas the second reduction process is much less affected (~10-20 mV), consistent with the assigned order of ligand reductions.

$[Ru^{II}(N^N^N)(N^N)(Cl)]^+$ complexes exhibit a slightly more complicated electrochemical behavior. Indeed, for most of the complexes within the series, neither of the two reductive features displays a significant reversibility. Moreover, the electrochemical signature from a new species appears upon reversing the sweep anodically. By comparison, this new oxidation wave can be assigned to the formation of the corresponding $[Ru^{II}(N^N^N)(N^N)(CH_3CN)]^{2+}$ complex, generated by Cl^-/MeCN exchange induced by the reduction. Inverting scan direction directly after the first reduction process provides more detailed information concerning the Cl^- lability within the series of complexes (Figures S33-40 in the Supplementary Information). In most cases, partial reversibility of the $[Ru^{II}(N^N^N)(N^N)(Cl)]^{+/0}$ couple is reached, leading to the simultaneous occurrence of reoxidation processes associated with the MeCN- and Cl^--bearing compounds. Increasing scan rates from 50 mV s^{-1} to 300 mV s^{-1} allows for reversibility improvement and reduced contribution from the acetonitrile derivative. Compounds **5-Cl** and **7-Cl**, however, exhibit a completely restored reversibility at all scan rates. This specific behavior strongly suggests that double reductions of these compounds are required before the chloride ligand is fully exchanged by a solvent molecule, indicating a lower Cl^- lability in **5-Cl** and **7-Cl**.

In order to extend our understanding of the electrochemical behavior of this family of compounds, diffusion coefficients were determined. According to the Randles-Sevcik equation, the slope associated with the linear plot of the Ru^{III}/Ru^{II} peak currents (i_{pa} and i_{pc}) as a function of the square

root of the scan rate was used to extract such diffusional data (Figure S41). Diffusion coefficients values ranging from 5 to $10*10^{-6}$ $cm^2.s^{-1}$ (Table S2) were obtained. Although chloride- and acetonitrile-bearing complexes differ in terms of overall charge, no clear trend can be distinguished. Similarly, plots of the anodic and cathodic peak potentials as a function of the logarithm of the scan rate were used to provide further details on the kinetics of the heterogeneous electron transfer process associated with the Ru^{III}/Ru^{II} process.[32] Typically, equivalent slopes of opposite signs (ranging from 10 to 15 $mV.dec^{-1}$) were observed (Figure S42), indicating a mostly symmetric energy barrier for electron transfer ($\alpha = 0.5$).

UV-Vis absorption spectra.

The UV-Vis absorption spectra of the $[Ru^{II}(N\text{^}N\text{^}N)(N\text{^}N)X]^{n+}$ (X = Cl^- / MeCN, n = 1 / 2) series of compounds were recorded in acetonitrile. Summarized in Table S3, spectroscopic data are typical of ruthenium(II) polypyridyl complexes, with intense absorption bands around 300 nm, attributed to ligand-centered $\pi-\pi^*$ transitions, and a broad metal-to-ligand charge transfer (MLCT) transition in the visible region. Plotting the energy of the absorption maximum as a function of the energy difference between the first ligand-centered reduction and metal-centered oxidation leads to a linear correlation (Figure S43, Supplementary Information). This result is in good agreement with the fact that in ruthenium(II) polypyridyl complexes, the molecular orbitals involved in the MLCT absorption are usually the same than those involved in the first reduction and oxidation processes.

One- and two-electron reduced states characterizations.

In order to provide detailed information on the nature of the catalytically relevant reduced states of this family of compounds, chemical reduction was performed on **1-MeCN** – a representative complex within the series. Titration of **1-MeCN** by decamethylcobaltocene, $Co(Cp^*)_2$, in dry DMF was monitored by UV-Vis spectroscopy (Figure 2). Differential absorption spectra have been calculated and are included to facilitate tracking of the most significant spectroscopic changes. Upon progressive addition of one equivalent of reductant (Figure 2, from black trace to red trace), three main features can be clearly identified: (i) the disappearance of the MLCT band at 455 nm, (ii) the rise of a strongly absorbing transition at 355 nm and (iii) the appearance of new broad transitions in the visible domain that culminate at 507 and 617 nm, respectively. These spectral modifications are associated with clear isosbestic points at 423 and 472 nm, indicating that no secondary reactions occur over the course of the measurement. Adding a second equivalent of $CoCp^*_2$ (Figure 2, from red trace to blue trace) results in the appearance of two new features at 321 nm and 555 nm. These results, and in particular the appearance of distinctive bipyridyl-type radical anion absorption at 355 nm and around 510 nm, share similar features to those obtained by UV-Vis spectroelectrochemistry of the complex $[Ru(bpy)_3]^{2+}$ that has clearly established the ligand-centered nature of the first two reduction processes.[33] Low-temperature EPR of the chemically generated one- and two-electron reduced species

of **1-MeCN** were then conducted. The EPR spectrum of the one-electron reduced species $[Ru(tpy)(bpy)(MeCN)]^{+}$, recorded at 10 K in acetonitrile, displays an weakly anisotropic signal with a *g*-value of 1.996 and 2.006 that is typical of organic radicals (Figure S44). Further reduction of **1-MeCN** to yield the two-electron-reduced $[Ru(tpy)(bpy)(MeCN)]^{0}$ complex reveals a rhombic EPR signal wit *g*-values of 1.973, 2.000 and 2.012 (Figure S45). While not being characteristic of an organic biradical, this signal might support the formation of a direduced species with either an anisotropic exchange interaction or a weak hyperfine interaction leading to the broadening of the EPR lines. These results are in good agreement with similar measurements performed on the reduced forms of $[Ru(bpy)_3]^{2+}$ and further strengthen our ligand-based reduction assignments.[34]

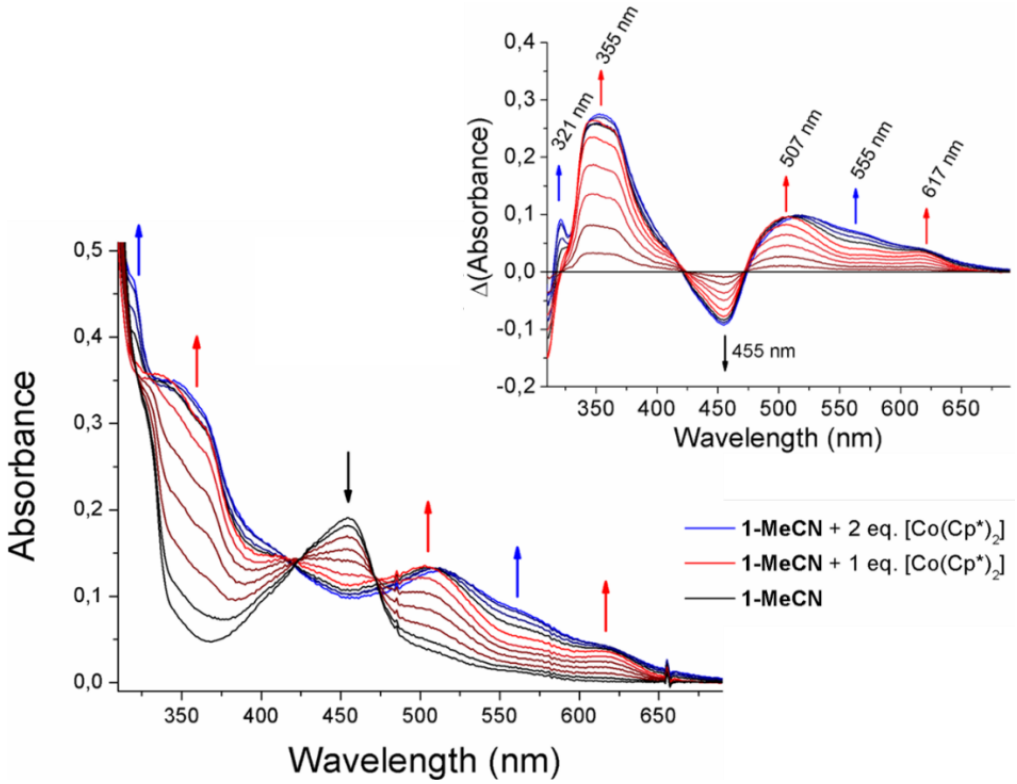

Figure 2. Evolution of **1-MeCN** UV-Vis spectrum upon progressive addition of $Co(Cp^*)_2$: from no added reductant (black trace) to one equivalent of $Co(Cp^*)_2$ (red trace) and two equivalents of $Co(Cp^*)_2$ (blue trace).

In an effort to more precisely describe the electronic structures of the different reduced states of **1-MeCN**, quantum chemical calculations were conducted. Not surprisingly, the DFT-optimized geometry of **1-MeCN** reveals a distorted octahedral coordination. Upon progressive reduction, the Ru-N bonds remain mostly unaffected whereas a contraction of the C-C bridging bonds of the polypyridyl ligands is observed (Figure S46). These results are in good agreement with experimental observations on the ligand-centered nature of the two successive one-electron reduction processes. The one-electron reduced complex **1-MeCN**$^{-}$ can be best described as a Ru^{II} complex bearing a radical-containing ligand with a doublet ground spin state (S = 1/2). The contour plot of the related singly occupied molecular orbital (SOMO) indeed displays a dominant bipyridine-based character (Figure 3A). The terpyridine ligand also partially contributes to this molecular orbital while the Ru 3d orbitals

involvement is very limited (< 5%). The two-electron reduced species, **1-MeCN**$^{2-}$, is characterized by an triplet ground spin state (S=1, Table S4, Figure S47) that adequately describes its biradical nature. Once again, the two calculated SOMOs are delocalized π* orbitals predominantly distributed on the polypyridine framework (Figure 3B-C). The effect of substituting the acetonitrile by a chloride ligand on the electronic structure of the system was also studied (Figures S48-49, Table S5). No major modification in the nature of the orbitals involved was identified.

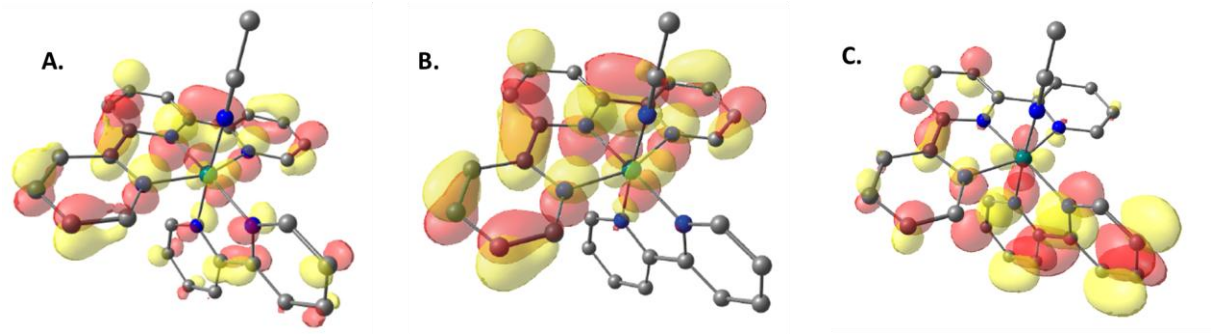

Figure 3. Localized SOMOs for (A) the one-electron reduced complex **1-MeCN**$^{-1}$ and (B-C) the two-electron reduced complex **1-MeCN**$^{-2}$.

The use of molecular catalysts favoring an electronic delocalization over the whole ligand is a strategy with wide interest in the case of electro-assisted CO_2[35-38] or proton[29, 39-41] reduction. However, some studies have also shown that redox involvement of the ligand can sometimes be deleterious by initiating some unwanted reaction pathways[42, 43] or excessive lowering of the metal center nucleophilicity.[44, 45] Knowing how to recognize these redox-active ligands and identify their characteristic spectroscopic signatures is therefore of great importance.

Conclusion.

Polypyridyl ruthenium(II) complexes of the type $[Ru^{II}(N\text{^}N\text{^}N)(N\text{^}N)(MeCN)]^{2+}$ have been prepared and fully characterized. The one- and two-electron reduced species of a representative complex within the series were spectroscopically investigated, providing relevant features to track these two species throughout various catalytic processes (hydrogen evolution or CO_2 reduction, as examples). Computational studies provided a comprehensive understanding of the evolution of the electronic structure of the complex upon the successive reductions. These results provide key spectroscopic features to enable future mechanistic studies and shed light on the importance of ligand-centered electronic processes.

Acknowledgements.

This work was supported by the Foundation Olle Engkvist Byggmästare (grant 2016/3), the Swedish Energy Agency (Grant no. 11674-8) and the NordForsk network NordCO_2. N. Q. also thanks Dr Vincent Maurel for fruitful discussions regarding this study.

References.

1. J. D. Knoll, B. A. Albani, C. B. Durr and C. Turro, *The Journal of Physical Chemistry A*, 2014, **118**, 10603-10610.
2. L. M. Loftus, K. F. Al-Afyouni, T. N. Rohrabaugh, J. C. Gallucci, C. E. Moore, J. J. Rack and C. Turro, *The Journal of Physical Chemistry C*, 2019, **123**, 10291-10299.
3. J. K. White, R. H. Schmehl and C. Turro, *Inorganica Chimica Acta*, 2017, **454**, 7-20.
4. J. Liu, C. Zhang, T. W. Rees, L. Ke, L. Ji and H. Chao, *Coordination Chemistry Reviews*, 2018, **363**, 17-28.
5. L. N. Lameijer, D. Ernst, S. L. Hopkins, M. S. Meijer, S. H. C. Askes, S. E. Le Dévédec and S. Bonnet, *Angewandte Chemie International Edition*, 2017, **56**, 11549-11553.
6. W. Sun, Y. Wen, R. Thiramanas, M. Chen, J. Han, N. Gong, M. Wagner, S. Jiang, M. S. Meijer, S. Bonnet, H.-J. Butt, V. Mailänder, X.-J. Liang and S. Wu, *Advanced Functional Materials*, 2018, **28**, 1804227.
7. M. Frasconi, Z. Liu, J. Lei, Y. Wu, E. Strekalova, D. Malin, M. W. Ambrogio, X. Chen, Y. Y. Botros, V. L. Cryns, J.-P. Sauvage and J. F. Stoddart, *Journal of the American Chemical Society*, 2013, **135**, 11603-11613.
8. S. Bonnet, J.-P. Collin and J.-P. Sauvage, *Inorganic Chemistry*, 2006, **45**, 4024-4034.
9. M. Hirahara, H. Goto, R. Yamamoto, M. Yagi and Y. Umemura, *RSC Advances*, 2019, **9**, 2002-2010.
10. N. Kaveevivitchai, R. Zong, H.-W. Tseng, R. Chitta and R. P. Thummel, *Inorganic Chemistry*, 2012, **51**, 2930-2939.
11. L. Tong and R. P. Thummel, *Chemical Science*, 2016, **7**, 6591-6603.
12. J. L. Boyer, D. E. Polyansky, D. J. Szalda, R. Zong, R. P. Thummel and E. Fujita, *Angewandte Chemie International Edition*, 2011, **50**, 12600-12604.
13. B. A. Johnson, S. Maji, H. Agarwala, T. A. White, E. Mijangos and S. Ott, *Angewandte Chemie International Edition*, 2016, **55**, 1825-1829.
14. Z. Chen, C. Chen, D. R. Weinberg, P. Kang, J. J. Concepcion, D. P. Harrison, M. S. Brookhart and T. J. Meyer, *Chem Commun (Camb)*, 2011, **47**, 12607-12609.
15. Z. Chen, P. Kang, M.-T. Zhang and T. J. Meyer, *Chemical Communications*, 2014, **50**, 335-337.
16. H. Nagao, T. Mizukawa and K. Tanaka, *Inorganic Chemistry*, 1994, **33**, 3415-3420.
17. H. Konno, A. Kobayashi, K. Sakamoto, F. Fagalde, N. E. Katz, H. Saitoh and O. Ishitani, *Inorganica Chimica Acta*, 2000, **299**, 155-163.
18. Z. Chen, C. R. K. Glasson, P. L. Holland and T. J. Meyer, *Physical Chemistry Chemical Physics*, 2013, **15**, 9503-9507.
19. Y. Matsubara, K. Koga, A. Kobayashi, H. Konno, K. Sakamoto, T. Morimoto and O. Ishitani, *Journal of the American Chemical Society*, 2010, **132**, 10547-10552.
20. T. A. White, S. Maji and S. Ott, *Dalton Transactions*, 2014, **43**, 15028-15037.
21. Z. Chen, J. J. Concepcion, M. K. Brennaman, P. Kang, M. R. Norris, P. G. Hoertz and T. J. Meyer, *Proceedings of the National Academy of Sciences*, 2012, DOI: 10.1073/pnas.1203122109.
22. B. P. Sullivan, J. M. Calvert and T. J. Meyer, *Inorganic Chemistry*, 1980, **19**, 1404-1407.
23. T. Ben Hadda and H. Le Bozec, *Inorganica Chimica Acta*, 1993, **204**, 103-107.
24. K. Barthelmes, M. Jäger, J. Kübel, C. Friebe, A. Winter, M. Wächtler, B. Dietzek and U. S. Schubert, *Inorganic Chemistry*, 2016, **55**, 5152-5167.
25. B. A. Johnson, H. Agarwala, T. A. White, E. Mijangos, S. Maji and S. Ott, *Chemistry – A European Journal*, 2016, **22**, 14870-14880.
26. H. J. Jang, S. L. Hopkins, M. A. Siegler and S. Bonnet, *Dalton Transactions*, 2017, **46**, 9969-9980.
27. G. R. Fulmer, A. J. M. Miller, N. H. Sherden, H. E. Gottlieb, A. Nudelman, B. M. Stoltz, J. E. Bercaw and K. I. Goldberg, *Organometallics*, 2010, **29**, 2176-2179.
28. N. Elgrishi, K. J. Rountree, B. D. McCarthy, E. S. Rountree, T. T. Eisenhart and J. L. Dempsey, *Journal of Chemical Education*, 2018, **95**, 197-206.

29. N. Queyriaux, W. B. Swords, H. Agarwala, B. A. Johnson, S. Ott and L. Hammarström, *Dalton Transactions*, 2019, DOI: 10.1039/C9DT03461G.
30. H.-W. Tseng, R. Zong, J. T. Muckerman and R. Thummel, *Inorganic Chemistry*, 2008, **47**, 11763-11773.
31. N. Elgrishi, M. B. Chambers, X. Wang and M. Fontecave, *Chemical Society Reviews*, 2017, **46**, 761-796.
32. E. S. Wiedner and R. M. Bullock, *Journal of the American Chemical Society*, 2016, **138**, 8309-8318.
33. G. A. Heath, L. J. Yellowlees and P. S. Braterman, *Journal of the Chemical Society, Chemical Communications*, 1981, DOI: 10.1039/C39810000287, 287-289.
34. A. G. Motten, K. Hanck and M. K. DeArmound, *Chemical Physics Letters*, 1981, **79**, 541-546.
35. W. Nie and C. C. L. McCrory, *Chemical Communications*, 2018, **54**, 1579-1582.
36. X. Su, K. M. McCardle, J. A. Panetier and J. W. Jurss, *Chemical Communications*, 2018, **54**, 3351-3354.
37. X. Su, K. M. McCardle, L. Chen, J. A. Panetier and J. W. Jurss, *ACS Catalysis*, 2019, **9**, 7398-7408.
38. C. Cometto, L. Chen, P.-K. Lo, Z. Guo, K.-C. Lau, E. Anxolabéhère-Mallart, C. Fave, T.-C. Lau and M. Robert, *ACS Catalysis*, 2018, **8**, 3411-3417.
39. P. Wang, G. Liang, M. R. Reddy, M. Long, K. Driskill, C. Lyons, B. Donnadieu, J. C. Bollinger, C. E. Webster and X. Zhao, *Journal of the American Chemical Society*, 2018, **140**, 9219-9229.
40. W. R. McNamara, Z. Han, P. J. Alperin, W. W. Brennessel, P. L. Holland and R. Eisenberg, *Journal of the American Chemical Society*, 2011, **133**, 15368-15371.
41. T. Straistari, J. Fize, S. Shova, M. Réglier, V. Artero and M. Orio, *ChemCatChem*, 2017, **9**, 2262-2268.
42. L. Duan, G. F. Manbeck, M. Kowalczyk, D. J. Szalda, J. T. Muckerman, Y. Himeda and E. Fujita, *Inorganic Chemistry*, 2016, **55**, 4582-4594.
43. G. C. Tok, A. T. S. Freiberg, H. A. Gasteiger and C. R. Hess, *ChemCatChem*, 2019, **11**, 3973-3981.
44. N. Queyriaux, K. Abel, J. Fize, J. Pécaut, M. Orio and L. Hammarström, *Sustainable Energy & Fuels*, 2020, **4**, 3668-3676.
45. T. H. T. Myren, A. Alherz, T. A. Stinson, C. G. Huntzinger, B. Lama, C. B. Musgrave and O. R. Luca, *Dalton Transactions*, 2020, **49**, 2053-2057.